

CORROSION PIT TO FATIGUE CRACK TRANSITION METHODOLOGY FOR AA7075-T651 ALUMINUM ALLOY

Divakar Mantha
SAFE Inc.
Center for Aircraft Structural Life Extension
2354 Fairchild Drive, Suite 2J2A
USAF Academy, CO 80840
USA

Matthew J. Hammond
SAFE Inc.
3290 Hamal Circle
Monument, CO 80132
USA

Scott Fawaz
SAFE Inc.
3290 Hamal Circle
Monument, CO 80132
USA

ABSTRACT

Corrosion damage (pit) is a stress raiser that can have deleterious effects on the fatigue life of airframe structural components. A better understanding and method for modeling the corrosion pit to fatigue crack transition would greatly help the aircraft community. This paper presents the development of a standardized fatigue test method for the determination of the transition of a corrosion pit to fatigue crack in aluminum alloy AA 7075-T651 specimens. The standardized test method requires the development and validation of several sub-protocols (1) a pitting protocol to create a mechanically small (< 200 μm diameter) corrosion pit on the hole edge of the fatigue specimen (2) a spot welding protocol for attaching the direct current potential drop (dcPD) probes on either side of the corrosion pit for fatigue crack growth measurement (3) a dcPD fatigue test method applying a unique 10-4-6 marker band sequence to measure the fatigue crack growth and (4) a crack growth life prediction protocol using AFGROW. AFGROW simulations are used to predict the crack shape evolution during the test. New stress intensity factor (SIF) solutions for small finite width plates with different crack shapes are being developed and validated with the pit-crack test sample for more accurate crack growth predictions.

Key words: Corrosion pit, Fatigue, AA7075-T651, AFGROW, Crack growth rate, Stress Intensity Factor

INTRODUCTION

Corrosion damage has a strong deleterious effect on the fatigue life of airframe structural components. Corrosion damage in the form of pits often occurs near rivet holes in the presence of environments such as humid air, salt water, and other harsh environments. Fatigue cracks often nucleate and grow

from corrosion pits as they act as stress concentrations. A standardized specimen and testing protocol to evaluate the relative influence of the environment, inhibitors and loading spectrum on the corrosion pit to fatigue crack transition is lacking. The transition of a fatigue crack from a corrosion pit is a complex process. Local macro- and micro-topography of a corrosion pit influence the transition from a corrosion pit to fully formed (continuous crack front from the plate surface to hole bore) fatigue crack. It is often assumed in aircraft damage tolerance analysis that the majority of fatigue life of a component is consumed before the crack is 1.27 mm in length. Therefore, understanding the transition from a corrosion pit on the order of 200 μm to a mechanically small crack is very important. This transition occurs in a region (< 1.5 mm) where most stress intensity solutions for crack geometries have not been validated.

The present investigation deals with the development of a standardized test method to determine the corrosion pit to fatigue crack transition in AA 7075-T651 specimens with a central hole. The development and validation of several intermediate procedures leading up to the standardization are also discussed. To aid the crack growth prediction in the small crack region, new stress intensity factor (SIF) solutions for finite width plates with different crack front scenarios are being developed.

EXPERIMENTAL PROCEDURE

Legacy aluminum alloy and heat treat (AA 7075-T651), Al-Zn-Mg-Cu alloy 7075 (Al - 5.7 Zn - 2.53 Mg - 1.66 Cu - 0.263 Fe - 0.06 Si - 0.026 Mn - 0.19 Cr - 0.02Ti; wt.%) in the peak aged T651 temper (24 hrs at 120 °C) obtained from the DARPA Structural Integrity Prognosis System (SIPS) program is used in this study [1]. Mechanical properties of this alloy are: tensile yield strength (σ_{ys}) was 508 MPa and plane strain fracture toughness (K_{IC}) in the longitudinal-transverse (L-T) orientation was 33 MPa $\sqrt{\text{m}}$. Figure 1 shows the specimen design and dimensions as well as the corrosion pit dimensions. All the dimensions shown in the figure are in millimeters (mm). For each specimen the flaw to nucleate the fatigue crack was a small controlled corrosion pit (< 0.2 mm diameter) inserted at the edge of the bore hole. Copper wires (0.127 mm diameter) which are used as potential probes are spot welded on each side of the corrosion pit by means of an in-house spot-welding setup. The sample was then loaded into a computer-controlled servo-hydraulic test frame and tested using a direct current potential drop (dcPD) system to monitor crack growth [3]. The dcPD method coupled with load induced marker bands are used to measure the fatigue crack growth. A fatigue crack was propagated from the pit until the crack reached approximately 1.5 mm in length, and then the test was terminated and the sample pulled to failure by static overload. The procedures involved in generating the corrosion pit followed by the spot-welding of probe wires are given below:

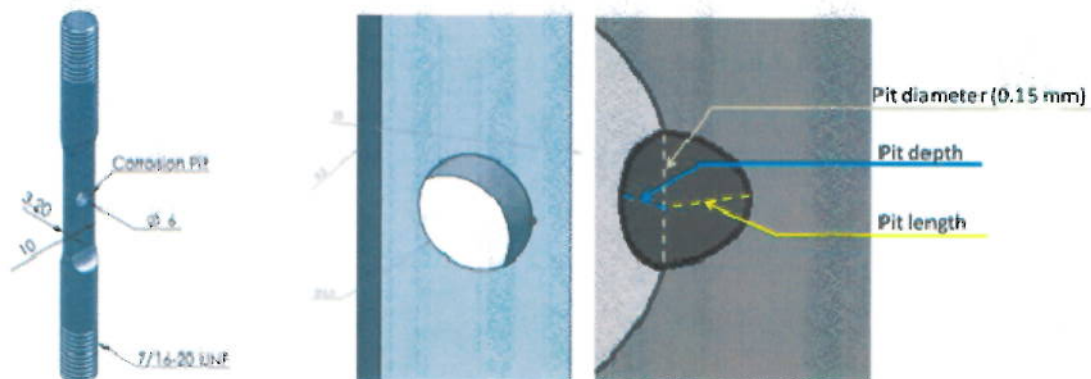


Figure 1: Specimen geometry and corrosion pit with dimensions.

Pitting Protocol

The specimen is held at an angle on a stand such that both surfaces (flat surface and curved surface of hole bore) of hole edge are clearly visible. The portion of specimen near the center hole is cleaned with isopropanol to remove any dirt. A 0.2 mm diameter hole is made by using a drill bit in an acid-resistant tape (0.107 mm thick) with dimensions of (9 mm × 2 mm). This tape with hole is carefully placed on the hole edge by means of tweezers such that both metal surfaces are visible through the tape's hole. Care must be taken to ensure that the tape's hole is clear of tape debris or glue. The specimen (except at the tape's hole) is masked with a non-reactive coating and dried for one hour. Corrosion pitting of the specimen takes place in a pitting solution (0.1 M AlCl_3 + 0.86 M NaCl with HCl added to make the pH 2) with a two-electrode corrosion setup. A very low constant current of 0.2 mA is passed for a prescribed time (1.5 min), obtained per Faraday's law calculations [4]. Since the tape's hole is very small, the pitting solution needs to be circulated using a peristaltic pump and directed toward the hole in the specimen. The specimen is removed from the solution, cleaned with water and placed under an optical microscope to observe the corrosion pit. A dark region in the tape's hole indicates the formation of a pit. The tape and coating are removed and the specimen is cleaned with water and then ultrasonically cleaned in isopropanol for 15 min. Figure 2 shows images of tape's hole and corrosion pit on the specimen. The complete corrosion pitting protocol is published elsewhere [5].

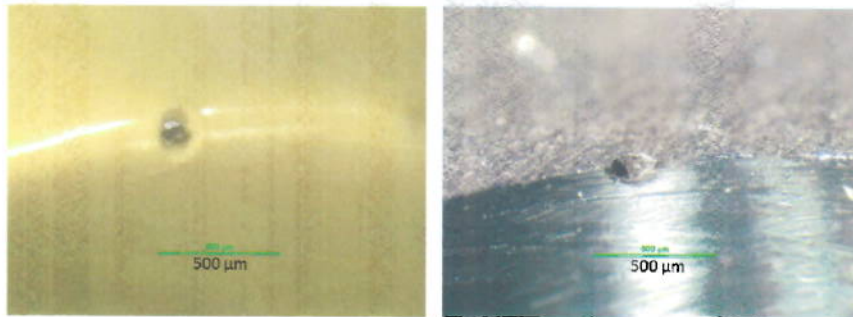


Figure 2: Example of tape placement at specimen hole edge and corrosion pit on AA 7075-T651 specimen.

Micro-topography of corrosion pit.

A scanning electron microscope (SEM) is used to study the micro-topography of corrosion pits. A HIROX digital microscope is used to measure the pit dimensions. Figure 3 shows an example of a HIROX and an SEM image of a corrosion pit.

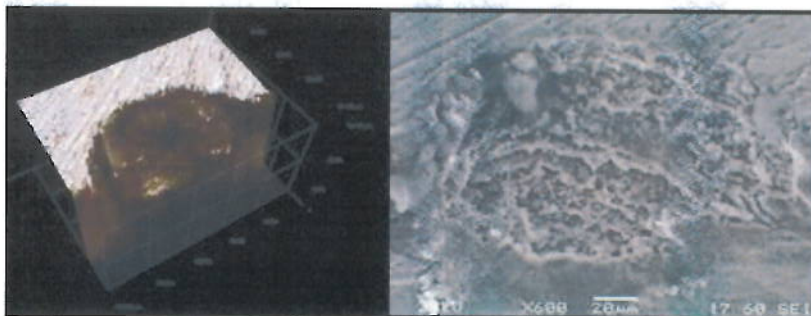


Figure 3: Example of a HIROX (left) and SEM (right) image of a corrosion pit on an AA7075-T651 specimen.

Spot-welding Protocol

The specimen with a corrosion pit is now ready for spot-welding of potential probes for the dcPD crack growth monitoring. Polytetrafluoroethylene (PTFE) insulated pure copper wires (0.127 mm diameter) are used as potential probes. The copper wires are spot-welded on each side of the corrosion pit equidistant from the pit centerline. The spot welding process is accomplished by an in-house designed and manufactured spot-welding setup that uses a Miyachi Unitek Corporation stored energy source with a portable head piece that holds the welding electrode (tungsten insert in Cu-Cr alloy shank). Figure 4 shows the spot welding stage with various components of welding. Two copper wires (0.6 m long) are stripped of their PTFE insulation at one end and are held in place guided by the wire positioning pulley grooves and thumb screws. The wire positioning pulleys allow for the precise spacing between the copper wires on each side of the corrosion pit. Prior to engaging the welding electrode the specimen is viewed through a microscope for precise placement of the electrode on the copper wire.

An optimum energy level was determined from earlier trial experiments such that a single stable weld joint can be made on each of the copper wires. It is very important to carefully place the wires such that the PTFE insulation of the un-stripped copper wire is as close as possible to the corrosion pit. This will ensure that only a very small portion of the bare copper wire away from the weld joint is left in contact with the alloy surface beneath. After welding, the two copper wires are carefully cut with a razor blade at the weld joints. The bare portion of the copper wire away from the weld joint is coated with a liquid insulation tape so that the potential probes (copper wires) are free from any electrical contact with the alloy specimen except at the spot weld regions. Figure 5 shows the example of wire placement, weld joints, and electrically insulated weld joints. The complete spot welding procedure is published elsewhere [6].

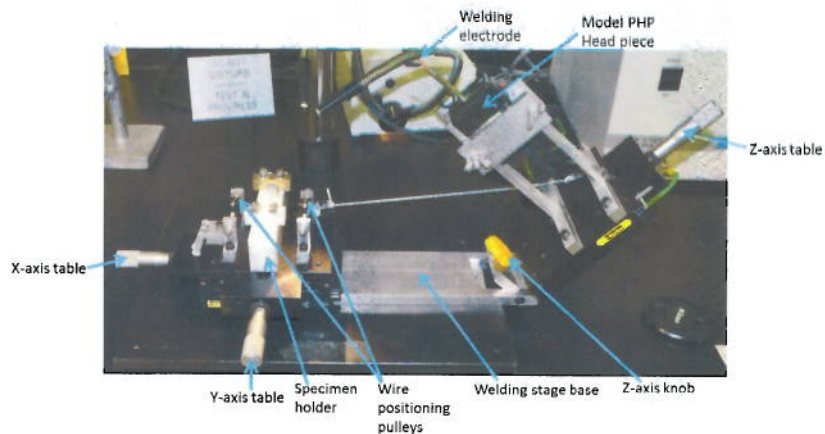


Figure 4: Spot welding stage showing various components of welding.

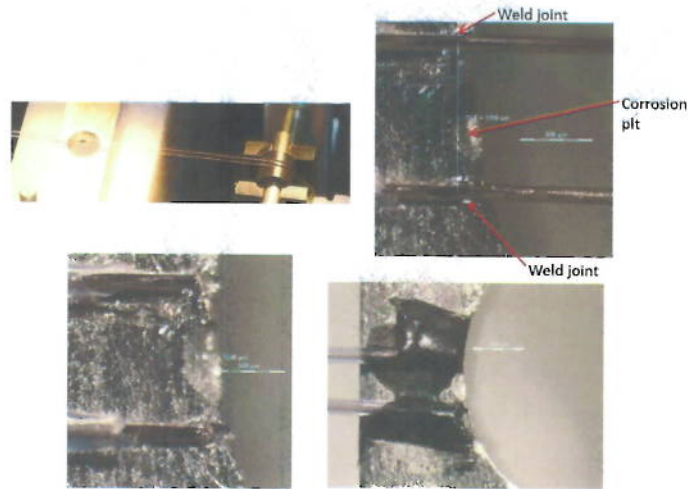


Figure 5: Examples of wire spacing, weld joints and electrically insulated weld joints on an AA7075-T651 specimen.

Fatigue Test

The principle of the dcPD method of monitoring crack length is that the electrical resistance of a cracked body changes with crack length. On application of constant current to a specimen, the change in electrical resistance results in a change of potential drop between the two measuring points (potential probes) across the crack. A closed-form analytical model was used to relate the measured potential to the crack length as a function of crack shape, probe position and probe spacing relative to the growing crack.

Variable amplitude fatigue test on an AA 7075-T651 specimen in lab air (shown in Figure 1) with a corrosion pit of pit length (c): 0.220 mm and pit depth (a): 0.180 mm is described in this paper. The spacing between the potential probe wires spot-welded on either side of the corrosion pit is 1.063 mm. The sample was then loaded into a computer-controlled servo-hydraulic test frame and tested using a direct current potential drop (dcPD) system. A constant current of 10 A is passed through the specimen from a dedicated power supply and amplifier. A unique 10-4-6 marker band loading spectrum [7] is introduced into the loading sequence to determine the evolution of the crack shape by post-test crack dimension measurements. The fatigue testing was conducted and test data are stored by means of the Automatic Fatigue Crack Growth Software provided by Fracture Technology Associates (FTA) [8]. The specimen dimensions and loading conditions are input into the FTA software prior to the test. In order to establish the initial voltage of the corrosion pit, the specimen is subjected to constant amplitude loading cycles at a very low load such that a crack does not nucleate. The dcPD signal was observed over time to ensure sufficient signal stability. It is well known that the electrical conductivity of aluminum alloys is acutely sensitive to temperature [3, 8]. To ensure sufficient stability of voltage signal both due to specimen heating and mechanical stability due to surroundings, the dcPD signal was observed over time prior to the fatigue test. The stabilization of dcPD signal (voltage) is achieved during constant amplitude cycling at low load. Typically, the stabilization of dcPD voltage can be achieved in one hour. Stabilization of dcPD signal is indicated by the signal fluctuation within $\pm 0.01 \mu\text{V}$ which is considered adequate for crack growth detection. After establishing the initial voltage for the corrosion pit, the specimen is tested at a maximum applied remote stress of 120.7 MPa, stress ratio (R) = 0.65, and a frequency of 5 Hz with the marker band loading spectrum. At the beginning of the test, the dcPD voltage shows transient readings prior to the crack growth. The transience of dcPD voltage can be attributed to the sudden increase in remote applied stress (P_{max}) on the specimen. The voltage corresponding to the corrosion pit can be obtained by averaging the voltage signal prior to the crack growth. The crack nucleation is identified when the dcPD voltage signal crosses a threshold value. The

threshold value for the current specimen dimensions and potential probe spacing is given by a normalized voltage ratio (V/V_0) of 1.002, where V_0 and V are the initial and instantaneous dcPD voltages respectively. The voltage signal clearly rises after crossing the threshold value indicating crack growth. A steep rise in the dcPD voltage is indicative of the crack becoming a fully formed (continuous crack front from the plate surface to hole bore) fatigue crack. The test was terminated when the crack in the specimen width direction reached approximately 1.5 mm in length and the sample was pulled to failure by static overload.

RESULTS AND DISCUSSION

The fatigue tested sample was analyzed for marker band locations using the SEM and the corresponding crack growth pattern was plotted. Figure 6 shows the dcPD voltage versus cycles for the entire fatigue test. The discontinuities (indicated by arrows in the figure) seen in the curve correspond to the marker band loading cycles during the test.

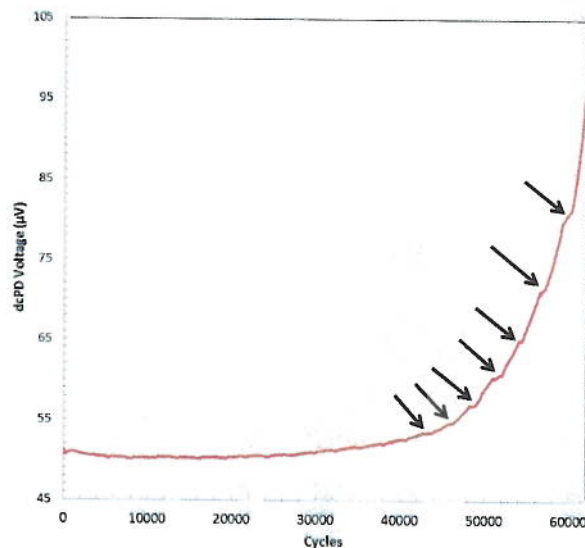


Figure 6: Direct Current Potential Drop (dcPD) voltage as function of cycles.

Crack Shape Evolution

Post-test analysis of the fractured surface using an SEM reveals the crack shape evolution with time from the known defect (corrosion pit) to the final crack length of 1.5 mm. Since the crack originates at the corrosion pit which is at a corner of the center hole of the specimen, the crack propagates in two directions along the hole surface 'a' and outer surface 'c'. Figure 7 (a) shows the SEM image of the fractured surface showing the corrosion pit and the final fatigue test boundary and (b) shows the marker band profiles during crack propagation. The specimen reached the final crack length limit of 1.5 mm after 61,924 cycles. Each "10-4-6" marker band loading constitutes 8,170 cycles. A total of 7 complete "10-4-6" marker band loading spectrums and one 10 marker were programmed during the fatigue test before the final crack length was reached. The post-test fractography by SEM revealed the crack propagation by means of marker band profiles which are shown in Figure 7(b).

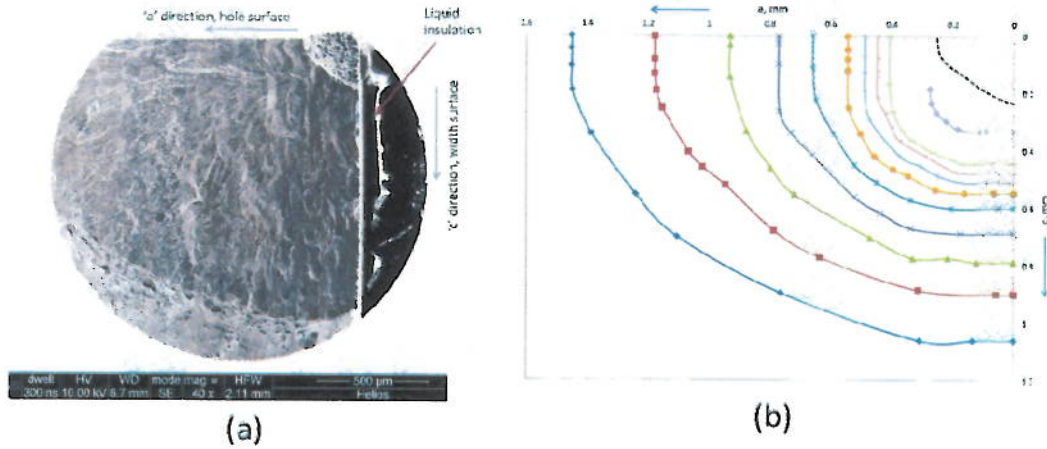


Figure 7: SEM image of the fractured surface and marker band profiles of crack shape evolution.

Table 1 lists the experimental crack growth data obtained from the marker band measurements using the SEM. The first column refers to the programmed marker type number, ex. 5th 10 marker, 5th 4 marker, etc. The outermost marker band in Figure 7(b) refers to 8th 10 marker followed by 7th 6 marker, then 7th 4 marker and so on. The table lists the crack dimensions (a, c) at different marker types that were identified unambiguously as periphery cracks (crack profiles that connect to the both ends). The innermost profile (dashed line in Figure 7(b)) refers to the outline of corrosion pit. Figure 8 shows the experimental crack length (c) 'red squares' and crack depth (a) 'black circles' as a function of cycles as obtained from the SEM analysis of marker band locations.

**Table 1
Experimental crack growth data**

Marker Type	Cycles, N	a, mm	c, mm	a/c
PIT	0	0.18	0.22	0.8182
5th 10	35225	0.2742	0.3338	0.8214
5th 4	37985	0.4075	0.4442	0.9174
5th 6	40525	0.4481	0.4772	0.9390
6th 10	43395	0.4888	0.5098	0.9588
6th 4	46155	0.5448	0.5475	0.9951
6th 6	48695	0.658	0.6006	1.0956
7th 10	51565	0.7711	0.6887	1.1196
7th 4	54325	0.9301	0.7886	1.1794
7th 6	56865	1.1783	0.8998	1.3095
8th 10	59735	1.4499	1.062	1.3653
END	61924	2.09	1.53	1.3660

Figure 9 shows the SEM images of the corrosion pit (left) and crack initiation sites (right) close to the flat surface ('c-direction') of the specimen. Figure 10 shows the plot of marker band profiles close to the corrosion pit (left) and the SEM image (right) indicating the locations of marker bands and crack that nucleated at the corrosion pit close to the hole bore surface of the specimen. The plot of marker band profiles (left) is oriented with c-direction as x-axis and 'a-direction' as y-axis so as to match the SEM image orientation. Further SEM analysis of the fracture surface near the corrosion pit reveals the crack nucleation site.

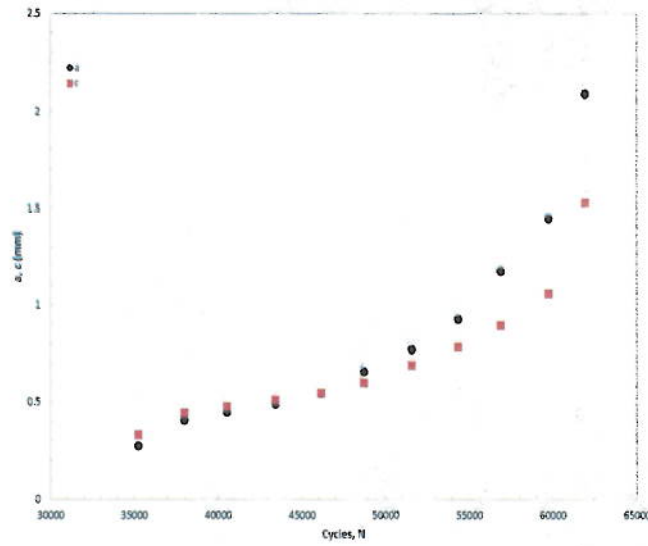


Figure 8: Experimental crack length (c) and depth (a) as a function of cycles.

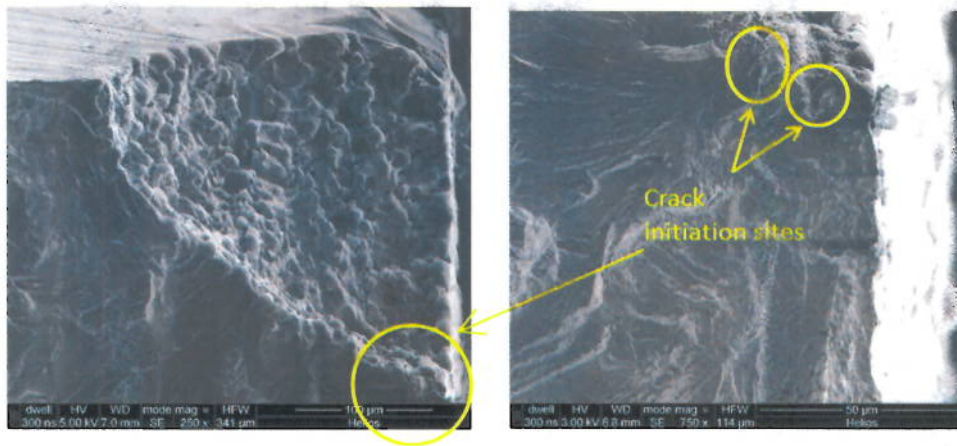


Figure 9: SEM images of corrosion pit (left) with initiation site and crack initiation sites (right) near the flat surface of the specimen.

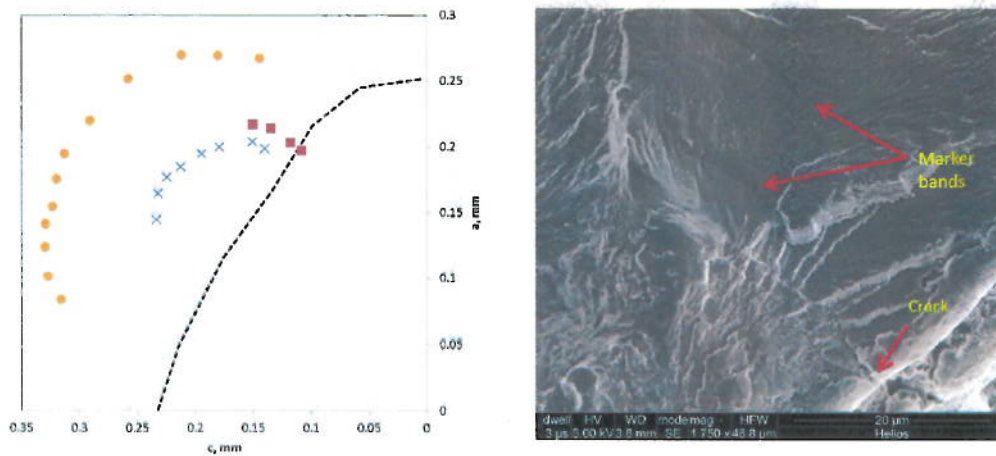


Figure 10: Marker band profiles (left) and SEM image of marker band locations and crack at the corrosion pit close to hole bore surface.

AFGROW Analysis and Crack Growth Rate Calculation

The crack growth based fatigue life is predicted using AFGROW [11]. AFGROW is a fracture mechanics and fatigue crack growth analysis software tool that allows crack initiation and growth to predict the life of metallic structures. The AFGROW corner crack K_I -solutions are used. The solutions are of the form given in equations (1) and (2):

$$K_a = \beta_a \cdot \sigma \sqrt{\pi a} \quad (1)$$

$$K_c = \beta_c \cdot \sigma \sqrt{\pi c} \quad (2)$$

Where K_a , K_c are the stress intensity factors, β_a , β_c are the geometric correction factors, σ is the remote applied stress and a , c are the crack depth and length, respectively. For any crack scenario, AFGROW predicts the two-dimensional crack growth (a , c) and provides K_a and K_c for the crack growth rate calculations. Stress intensity factors (SIFs) in both 'a' and 'c' directions for the experimental crack growth rates are obtained by interpolation using the DARPA structural integrity prognosis system (SIPS) database for AA7075-T651 at $R = 0.65$. Crack growth predictions were carried out using corrosion pit depth and length as the starting crack dimensions. The crack growth profiles can also be predicted using any crack front scenario (marker band location of a periphery crack).

An analytical relationship between measured electric potential and crack length was developed by Roe and Coffin [9] for a three dimensional ellipsoidal surface disturbance in an infinite plate. The influence of initial defect on near-defect crack monitoring was modeled for a specimen with a specific initial defect (corrosion pit) and potential probe dimensions [10]. Potentials corresponding to the AFGROW predicted crack growth profiles are obtained from the analytical solution.

Crack growth rates for the experimental data in both directions are calculated using the incremental polynomial method outlined in the Appendix X1.2 of the ASTM E647 [2]. Figure 11 shows the comparison between the experimental crack length and depth to those of dcPD calculated values. The calculated crack length and depth are normalized with respect to the initial pit dimension and final crack dimensions. The aspect ratio (a/c) of the crack was less than 1.0 at the beginning and exceeds 1.0 after 46,000 cycles. The calculated crack dimensions are in excellent agreement with the experimental crack dimensions. Figure 12 shows the crack growth rate in both directions as a function of the stress intensity factor range, ΔK . The corresponding data for the same alloy available from the SIPS database are also shown in the figure as a dashed line. The crack growth rate data of this specimen is in excellent agreement with that of the SIPS database except at higher ΔK values. The crack growth rates were similar in both the planar surface and along the hole bore direction ('c' and 'a' directions, respectively).

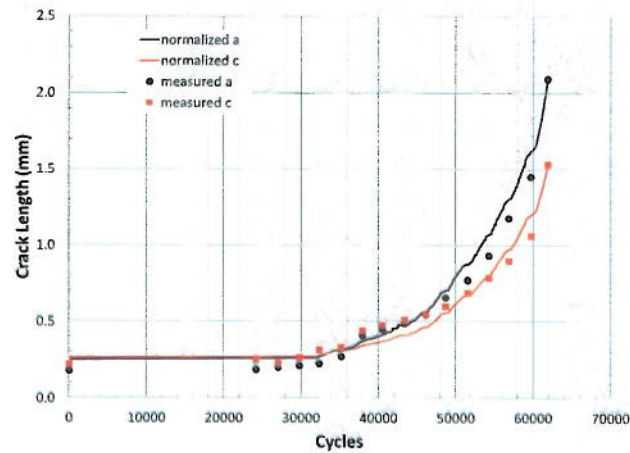


Figure 11: Comparison of calculated and experimental crack lengths (a, c).

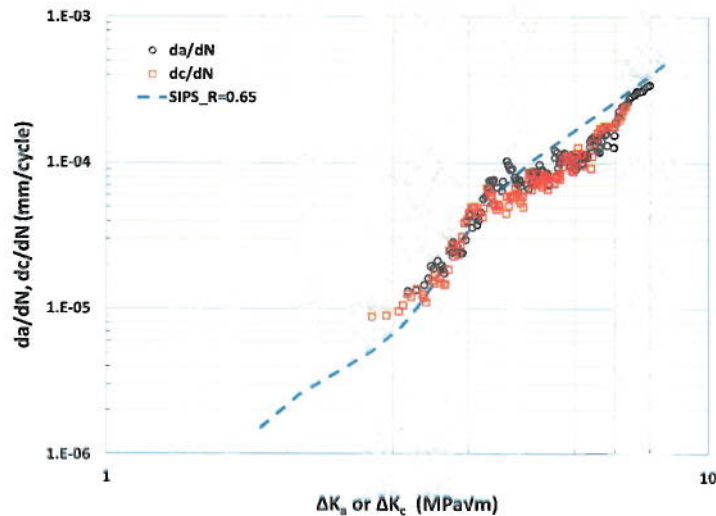


Figure 12: Crack growth rates as function of ΔK in both 'a' and 'c' directions.

New SIF Solutions

Comparisons between the test specimen and AFGROW predicted data show differences in the evolving crack shape (i.e. the crack-front aspect ratio, a/c) as a function of overall crack growth. Possible sources of these discrepancies could be, of many, the SIPS crack growth rate data and the SIF solutions. In an effort to resolve the discrepancies, new SIF solutions are being developed for the pit-to-crack specimen, which has extreme finite width effects, which are not properly accounted for in the current AFGROW simulations [11].

An example of the differences between the AFGROW and newly developed SIF solutions is shown in Figure 13. This example is for a fixed 'a' direction crack length with varying 'c' direction crack lengths, and thus varying crack aspect ratios. The solutions are presented as a function of the normalized parametric angle of an ellipse, ϕ , around the crack front, with 0 being the 'c'-tip and 1 the 'a'-tip. The Advanced ('Adv') AFGROW solutions are presented here with solid lines and the new solutions are presented as discrete points. As can be seen from Figure 13, there can be significant differences in the SIF value with varying crack geometry from the ones used in the current prediction models. Most significant is the large differences at the 'c'-tip (near an angle of 0) of the $a/c = 1.5$ data set, since the test specimen a/c values range from 0.82 to 1.37.

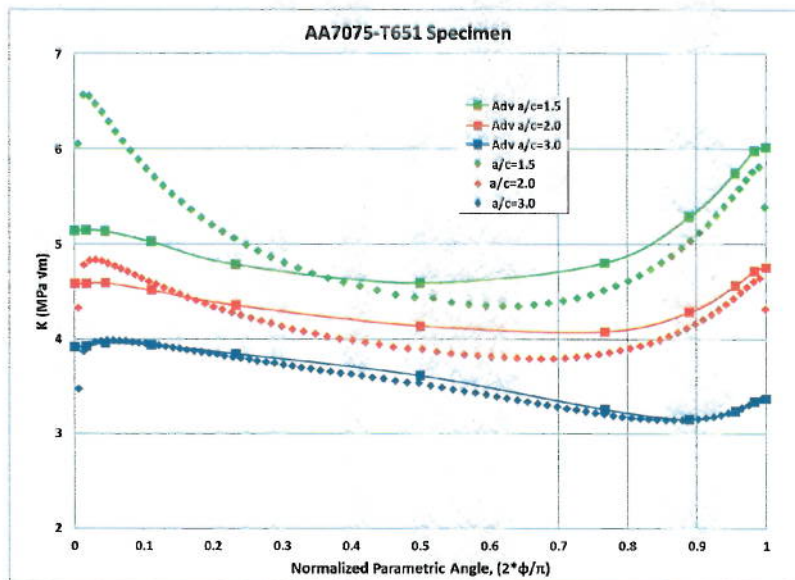


Figure 13: New SIF solutions for the AA7075-T651 specimen as a function of angle around the crack tip compared with current AFGROW solutions.

These analytical results warrant further investigation and a significant effort is underway to generate a high-fidelity solution space.

CONCLUSIONS

A laboratory procedure was developed and successfully demonstrated in introducing small corrosion pits (0.2 mm diameter) at center hole edge of an AA 7075-T651 specimen. A single stable weld joint of the potential probes was achieved. Fatigue life of AA 7075 aluminum alloy with an induced corrosion pit was determined. Post-test fractography revealed the crack nucleation sites close to the corrosion pit. Crack growth rates in both 'a' and 'c' directions as a function of stress intensity factor range are in excellent agreement with that of the SIPS database. However, better agreement may be obtained for the evolution of the crack shape through the application of the newly generated SIF solutions. These efforts may help the engineering community reach a better understanding of the mechanisms of and inhibitors to the transition of a corrosion pit to a crack.

ACKNOWLEDGEMENTS

This work is based on the research sponsored by the US Air Force Academy under agreement number FA7000-11-2-0011 of the Department of Defense Office of the Secretary of Defense.

The views and conclusions contained herein are those of the authors and should not be interpreted as necessarily representing the official policies and endorsements, either expressed or implied of US Air Force Academy or the US Government. Approved for public release, distribution is unlimited.

REFERENCES

1. J. T. Burns, J. M. Larson, and R. P. Gangloff, "Driving Forces for Localized Corrosion-to-Fatigue Crack Transition in Al-Zn-Mg-Cu," *Fatigue & Fatigue of Engineering Materials and Structures* 34 10 (2011): pp. 745-773.
2. ASTM E647, "Standard Test Method for Measurement of Fatigue Crack Growth Rates" (West Conshohocken, PA: ASTM), 2000.

3. R. P. Gangloff, D. C. Slavik, R. S. Piascik and R. H. Van Stone, "Small-crack Test Methods," *ASTM STP 1149*, Eds. J. M. Larsen and J. E. Allison, ASTM International, (West Conshohocken, PA, 1992), pp. 116–168.
4. D. A. Jones, *Principles and Prevention of Corrosion*, 2nd ed. (Upper Saddle River, NJ: Prentice-Hall, Inc., 1996).
5. USAFA-TR-2013-04, "Pitting Protocol," Center for Aircraft Structural Life Extension (CAStLE), USAF Academy, CO 80840.
6. USAFA-TR-2013-05, "Spot Welding Protocol," Center for Aircraft Structural Life Extension (CAStLE), USAF Academy, CO 80840.
7. S. Fawaz, "Fatigue Crack Growth in Riveted Joints," (Delft University, The Netherlands, 1997).
8. J. K. Donald and J. Ruschau, "Direct Current Potential Difference Fatigue Crack Measurement Techniques" In *Fatigue Crack Measurement: Techniques and Applications*, Eds. K. J. Marsh, R. A. Smith, and R. O. Ritchie, Engineering Materials Advisory Service Ltd., (Warley, UK, 1991), pp. 11-37.
9. G. M. Roe and L. F. Coffin, *Unpublished Research*, General Electric Corporate Research and Development (1978).
10. R. P. Gangloff, "Electrical Potential Monitoring of Crack Formation and Subcritical Growth from Small Defects," *Fatigue of Engineering Materials and Structures* 4 1 (1981): pp. 15-33.
11. www.AFGROW.net version 5.01.06.17 (May 2011).